



## Phase field approach for simulating failure of viscoelastic elastomers

Roberto Brighenti <sup>a,\*</sup>, Timon Rabczuk <sup>b</sup>, Xiaoying Zhuang <sup>c</sup>

<sup>a</sup> Department of Engineering & Architecture, University of Parma, Parco Area delle Scienze 181/A, 43124, Parma, Italy

<sup>b</sup> Institute of Structural Mechanics, Bauhaus University of Weimar, Marienstraße 15, D-99423, Weimar, Germany

<sup>c</sup> Institute of Continuum Mechanics, Leibniz Universität Hannover, Hannover, Germany

### ARTICLE INFO

**Keywords:**

Elastomers  
Polymers  
Damage  
Visco-elasticity  
Fracture  
Phase-field

### ABSTRACT

The description of a problem involving the existence of an interface or of a strong discontinuity requires to solve partial differential equations on a moving domain, whose evolution is also unknown, leading to severe difficulties, especially when the interface undergoes topological changes. The solution becomes even more complex when the whole problem domain changes, such as in mechanical problems involving large deformations. In this context, the phase-field approach allows to easily reformulate the problem through the use of a continuous field variable mimicking the real physical discontinuity. In the present paper we take advantage of such an approach for the description of damage and failure of highly deformable strain rate-dependent materials, such as the elastomeric ones. By harnessing a statistical physics-based micromechanical model of the polymers chain network characterized by the capability to reorganize the distribution of its chain lengths in time, the behavior of a rate-dependent polymer can be simulated. The adopted physics-based approach, upscaled at the continuum level and combined with a phase-field approach, allows us to describe the damage and fracture occurring in this class of materials in the large deformations regime. Some examples are provided to demonstrate the reliability of the proposed model.

### 1. Introduction

Many real physical problems involve a moving boundary or interface, whose shape and position has to be determined while solving the problem itself. All these problems share the common feature that their mathematical description requires the solution of partial differential equations (PDEs) within a moving domain, coupled to others PDEs describing the boundary conditions on an evolving interface. Just to mention some exemplificative cases, it's worth recalling problems involving multiphase flows, phase transformation in metallic alloys, phase solidification in pure materials, phase separation of binary systems, interdiffusion of alloys made of two components, growth in biological tissues, etc. (Provatas and Elder, 2011).

Based on a variational formulation of fracture firstly introduced by Francfort and Marigo (1998) – whose main feature is the minimization of the total energy of the system with respect to the geometry of the crack domain and the displacement field – in recent years a new method, known as phase field approach, has been developed.

The phase-field has shown the capability to efficiently describe discontinuous phenomena in different engineering and physics fields;

among the several tackled problems, it's worth mentioning the successful use of the phase-field for the simulation of the crack growth in brittle and cohesive materials (May et al., 2015), in anisotropic media (Nguyen et al., 2017), the dendritic growth in materials (Steinbach, 2009), for the study of the phase separation and dissolution processes (Miura, 2018; Amiri et al., 2019) and solidification phenomena (Song et al., 2018; Yu et al., 2018a), microstructure evolution (Chen, 2002; Li et al., 2017), multiphase fluid flow and capillarity problems (Steinbach, 2009; Miura, 2018; Amiri et al., 2019; Song et al., 2018; Yu et al., 2018a; Chen, 2002; Li et al., 2017; Jacqmin, 1999; Antanovskii, 1995), mechanics of shell membranes (Biben et al., 2005), and many others (Schmitz, 2017; Torabi et al., 2009).

Among the various problems involving the existence of a sharp interface, the fracture failure mechanism in materials can be seen as the process of creation of a free surface embedded in the body; this phenomenon has a highly discontinuous nature, since the arising displacement field results to be so, and the corresponding strains become unbounded at the crack location. In order to simulate efficiently the fracture process in materials, the phase-field approach, has been developed in the last decade and nowadays constitutes an efficient computational tool enabling to get satisfactory results to a wide range of

\* Corresponding author.

E-mail addresses: [brigh@unipr.it](mailto:brigh@unipr.it) (R. Brighenti), [timon.rabczuk@uni-weimar.de](mailto:timon.rabczuk@uni-weimar.de) (T. Rabczuk), [zhuang@ikm.uni-hannover.de](mailto:zhuang@ikm.uni-hannover.de) (X. Zhuang).

Nomenclature	
$b$	Kuhn's length of a chain segment
$\mathbf{b}, \mathbf{B}$	Volume force vector in the current and in the initial configuration, respectively
$c_{a0}, c_a(t)$	Number of active chains per unit volume in the initial stress-free state and at the generic time $t$ , respectively
$c_\mu = c_a(t \rightarrow \infty)$	Steady state value of the chain concentration
$\mathbf{E}$	Green-Lagrange deformation tensor
$f_{0,f}$	Normalized distribution function of the polymer's chains end-to-end vector in the stress-free and in the current state, respectively
$\mathbf{F}, F_{ij}$	Deformation gradient tensor
$G_c$	Fracture energy
$k_a, k_d$	Activation and deactivation reaction rates, respectively
$k_B$	Boltzmann's constant
$\mathbf{L}, L_{ij}$	Spatial velocity gradient
$\mathcal{L}, \mathcal{L}^{-1}$	Langevin function and its inverse, respectively
$N$	Number of segments in a polymer chain belonging to a single network
$p$	Hydrostatic stress
$\mathbf{r}$	End-to-end vector distance of a polymer chain
$\mathbf{P}$	First Piola stress tensor
$s$	Order parameter or phase-field parameter
$t$	Time
$\mathbf{t}$	Force in a single chain
$T$	Absolute temperature
$\mathbf{x}, \mathbf{x}$	Position vector of a generic point in the undeformed and in the deformed configuration, respectively
$\varepsilon$	Characteristic length of the phase field
$\phi_0(\mathbf{r}), \phi(\mathbf{r})$	Distribution function of the end-to-end vector in the stress-free and in the current state, respectively
$\dot{\phi}, \dot{\phi}_L, \dot{\phi}_V$	Time rate of the chain distribution function and of its deformation- and strain-rate dependent counterparts, respectively
$\Gamma_c$	Crack domain
$\lambda$	Macroscopic stretch and stretch of the polymer chains assumed to be identical according to the affine deformation hypothesis
$\mu$	Shear modulus
$\psi$	Deformation energy of a single chain
$\Psi_0, \Psi$	Network's deformation energy per unit volume in the stress-free and in the current configuration, respectively
$\Psi_b, \Psi_s, \Psi_e$	Internal energy of the material accounting for diffuse crack degradation, crack surface energy and external energy, respectively
$\sigma$	Cauchy stress
$\omega$	Deformation function
$\square = \int \square d\Omega$	Integral over the chain configuration space

physical problems involving complex fixed or evolving discontinuities (Zhou et al., 2018; Teichtmeister et al., 2016; Miehe and Schänzel, 2014; Gomez and van der Zee, 2018; Biner, 2017). The use of more complex but less general techniques, such as remeshing (Bouchard et al., 2000), the use of cohesive elements (Wells and Sluys, 2001) or the approaches based on the local enrichment of the displacement field (Zhang et al., 2016), can thus be avoided.

The main idea behind the phase-field approach, is the representation of the discontinuity domain (typically constituted by a line in 2D and by a surface in 3D problems) through a continuous mathematical description, provided by the so-called order parameter or phase-field (scalar) parameter. For instance, by considering the phase separation phenomenon of two substances A and B, such a parameter can be made to vary smoothly from two extreme values, namely 1 when at the considered point the material is completely made of the substance A and 0 if the point is located in a region made of the substance B. In all the intermediate cases in which the two substances are mixed in different proportions, the order parameter assumes values in between the two above-mentioned bounding values, leading to the so-called phase-field.

The application of this concept to fracture mechanics is straightforward; the two substances can be assumed to be represented by the unfailed material and by the ruptured one, the latter representing a fully damaged localized region, usually referred to as a crack. According to this theory, the total potential energy of the body is assumed to be provided by both the strain energy of the bulk material and by the surface crack energy playing the role of the energy required for crack initiation and propagation.

One of the key aspect of this continuous approach to fracture is the regularization of the discrete crack into a diffused entity, usually – as mentioned above – termed as the phase-field. In this way, theoretically infinite states of the material exist, falling between the fully cracked and the completely intact one. It is worth mentioning that, sometimes, in fracture mechanics the existence of a partially cracked material is postulated through the concept of the cohesive or process zone, originally postulated by Barenblatt (1962) and Dugdale (1960), existing ahead of the crack tip (Elices et al., 2002). In such a zone the stress field still exists (until the crack propagate further into that region) but is

weakened by the presence of the crack. The phase-field approach has been proven to be suitable to study the fracture in brittle solids, but has also been successfully applied to other classes of materials (Miehe and Schänzel, 2014); from this perspective, the phase-field can be seen as an extension of the above-mentioned cohesive model, and operates by introducing the concept of a partially cracked material not only in the region close to the crack tip but in the entire domain of the problem.

Thanks to its huge potentialities, within the fracture mechanics context the phase-field can be easily used to describe complex problems involving strong discontinuities, such as those arising in crack initiation and propagation, crack branching, crack coalescence, etc. without the need to use any special formulation nor adapting the domain discretization to the growing crack. From this perspective, it represents a very convenient approach to deal with a generic fracture process, especially in a three dimensional setting (Bhowmick and Liu, 2018a), it does not require to explicitly track the location of the crack surface and allows to deal with heterogeneous materials (Hansen-Dörr et al., 2018). From a mathematical viewpoint, the problem is governed by a coupled system of non-linear quasi-static or dynamic equilibrium equations, together with a gradient-type evolution equation for the crack phase-field (Kuhn and Müller, 2010).

The phase-field approach requires the introduction of a length regularization parameter, controlling the width of the intact-damaged transition zone, whose size heavily affects the mesh fineness required to resolve the high gradients arising close to the crack (Kuhn and Müller, 2011); this represent one of the major drawbacks of the method. Another issue arising when using this approach to solve problems with discontinuities, relies on the appropriate choice of the time step used for the integration of the quasi-static governing equations in the time-domain, which is typically required to be sufficiently small to ensure the computational stability of the solution.

The phase-field method has also been successfully applied to the fracture simulation of viscoelastic solids; for this class of materials, the time dependence is usually accounted for through a Maxwell-like approach and by accounting for the viscous energy dissipation in the crack driving energy balance, while the stress state is typically evaluated by considering the deformation history of the material through a

convolution integral approach (Yin and Kaliske, 2020; Shen et al., 2019).

Failure in polymers has been explained in the literature through phenomenological as well as physics-based approaches; among the first category, it is worth mentioning the so-called cavitation mechanism, which explains the damage occurrence to be originated from the expansion and growth of small existing cavities embedded in the bulk of the material (Gent and Wang, 1991; Fond, 2001; Lin and Hui, 2004; Lev and Volokh, 2016). It is has been well established that in elastomeric materials, regions having stress states characterized by a sufficiently large triaxiality values (i.e. regions of maximum tensile hydrostatic to deviatoric stress ratio) can induce the sudden appearance, expansion, growth and coalescence of internal cavities leading to a macroscopic flaw. The occurrence of such instabilities, commonly referred to as cavitation, can be attributed to the growth of pre-existing defects into finite size flaws. Since elastomers typically show an incompressible behavior and are characterized by a very low elastic modulus compared to the cohesive strength, they are sensible to tensile hydrostatic stress states (Lev and Volokh, 2016), and the damage mechanism can be recognized to take place through the growth of small existing voids which coalesce into greater macroscopic defect; this damage mechanism originates preferentially under hydrostatic tension (Lev and Volokh, 2016). This phenomenon can be framed within the fracture mechanics approach, by assuming the fracture energy as the decohesion energy of the material under a tensile hydrostatic stress (Cristiano et al., 2010).

On the other hand, physics-based micromechanical approaches have also been proposed to explain the damage occurrence in elastomers; within this class of models, the rupture of the polymeric chains at the microscale has been used to explain the damage observed in these materials at the meso-scale (Mohammadi et al., 1993; Hui et al., 2004). According to this approach, the fracture in polymers is the consequence of the collective failure of the network chains occurring through a chain scission mechanism; according to this approach, upon the attainment of the critical value of the bond stretching energy the single chain detaches from the network and does not contribute any more to the load bearing mechanism of the material (Talamini et al., 2018). From a continuum perspective, since in polymers the damage mechanism occurs while the material is behaving elastically (it is well-known it to occur also at high strain values), the energetic approach, initially proposed by Griffith, could be appropriate in these cases (Thomas, 1994).

Further, it is well-known that polymers and polymer-like materials show a time-dependent (or strain rate-dependence) response (Knauss, 2015), whose severity usually increases with the temperature; in this class of materials the crack growth rate is primarily related to the mechanism of viscous flow taking place close to the crack tip region and, because of the nearly incompressible response of polymers, the viscous response is mainly related to the deviatoric part of the deformation.

In this study we consider the strain rate behavior of polymers by adopting the concept of internal microstructural remodeling, i.e. by borrowing the ability of some polymers with dynamic cross-links (namely vitrimers, polymers with physical (ionic) bonds, etc.), to reset their chains' stretched state into the rest one (Yu et al., 2018b). This micromechanical model constitutes an alternative and quite different approach compared to the classical ones based on rheological models and enables to easily describe the time-dependent response of the material (on the basis of few physics-based parameters) without the need of any convolution integral to be evaluated over the time history experienced by the material (Long et al., 2013). For this class of materials we adopt a rate-dependent model based on the concept of network rearrangement at the microscale, together with a phase-field approach, to study the fracture process of viscoelastic polymers undergoing large deformation. Starting from a micro-mechanical based approach to the mechanics of amorphous materials (elastomers), we introduce the concept of chain network with dynamic bonds (dynamic cross-links) to simulate the stress relaxation taking place in strain-rate dependent materials.

The influence of the main aspects involved in the viscoelastic fracture phenomenon are taken into account, including the microstructure evolution velocity and the role played by the applied deformation rate. Some final examples are proposed to illustrate how the developed computational approach can be conveniently adopted to simulate the crack and damage evolution in strain-rate dependent polymers.

The outline of the paper is as follows: in section 2 we motivate the goal of the research by firstly illustrating the statistical-based approach to the mechanics of polymers through the use of the concept of the chain distribution function. In the same section, we consider the extension of the theory to deal with viscoelastic phenomena taking place in materials characterized by a network-like underneath structure. In section 3 we briefly introduce the phase-field approach for fracture problems and in section 4 we particularize the phase-field approach for the case of highly deformable materials, with a special emphasis on the elastomeric ones. Finally, section 5 is devoted to the illustration of some representative examples, while in section 6 we drawn some concluding remarks and perspective issues.

## 2. Statistical-based mechanics of network chains for viscoelastic polymers

Because of the thermal fluctuations taking place in their entangled network-like amorphous microstructure, the mechanics of polymers has been recognized to be mainly governed by entropic effects; the knowledge of the state of such a microstructure, suffices to fully know the state of the material. Such an entropic energy function can thus be used to describe the response of polymers and polymer-like materials, at least for not too large deformation levels since, when the chains are stretched nearly to their contour length, the enthalpic effect plays the main role while the entropic one becomes less important (Flory, 1953; Gordon, 1975).

The mechanics of polymers, can be developed by following the classical rubber elasticity theory that assumes the chain energy to depend only on the current distance existing between its two extremities (end-to-end vector distance  $\mathbf{r}$ ) jointed to other chains at discrete points termed as cross-links (Flory and Rehner, 1943), (Treloar, 1946). In polymeric materials such chain junctions can have different nature, ranging from strong covalent bonds to the weaker physical ionic ones.

The simplest polymer microstructure model (Doi, 1996) assumes the network to be made of an entangled arrangement of chains, each one made by  $N$  rigid segments of equal length  $b$  (Kuhn's segments), conformed according to the so-called random-walk theory and connected at their extremities to the network, while no correlation is assumed to exist between the segments' directions (freely-jointed chain model, FJC) (Fixman, 1972; Boyce and Arruda, 2000). Based on the chains-like nature of the network, several simple mechanical models for polymers have been proposed so far, such as the so-called 3-, 4-, 8-chains models (Boyce and Arruda, 2000) and the more general full-network model by Wu and van der Giessen (Wu and van der Giessen, 1993).

We adopt here a statistical-based approach to describe the mechanics of polymers (Flory, 1969), extended to account for the time-dependent effects; the above-cited micromechanical model, properly upscaled at the continuum level, is coupled to the variational-based phase-field approach, with the final aim to develop a physics-based model for describing the fracture process in elastomers. As mentioned above, the strain rate effects are also considered in order to quantify the stress relaxation taking place when sufficiently low strain rates are applied to the polymer. This phenomenon can be related to the chains rearrangement in time and is here modeled by adapting a recently proposed kinetic theory – describing the mechanics of polymers with dynamic bonds (Vernerey et al., 2017; Brighenti et al., 2019) – based on the internal microstructural re-arrangement of the chain network.

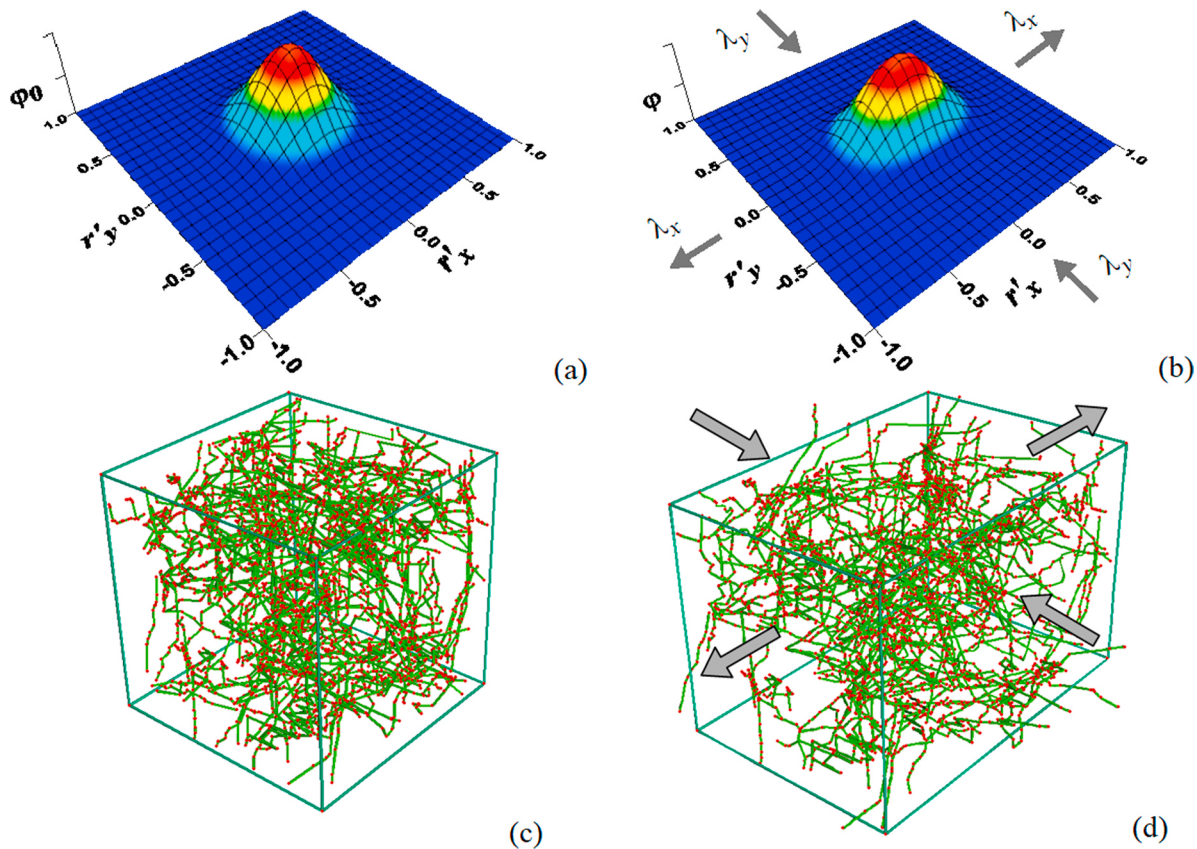


**Fig. 1.** Scheme of the chain distribution function in the reference configuration (a) and corresponding polymer network (c); chain distribution function (b) after stretching the polymer network in the  $x$  direction (d).

### 2.1. Statistical description of a polymeric network

The mechanical response of a polymer is strictly connected to the state of its underlying network, whose is reflected in its macroscopic behavior; from this viewpoint, the knowledge of the effects produced on the chain network by a generic deformation process, suffices to evaluate the state of the polymer at the macroscale. Since, according to the FJC model, the state of a polymer's chain is fully described by the knowledge of its chain' end-to-end vector  $\mathbf{r}$ , the statistical distribution of  $\mathbf{r}$  provides all the necessary information required to determine the stress state in the material. The end-to-end vectors distribution is provided by the function  $\phi(\mathbf{r})$ , hereafter indicated as the chains distribution function. In the reference (macroscopically stress-free) state it is indicated with

$$\phi_0(\mathbf{r}) = c_{a0} f_0(\mathbf{r}) \quad (1)$$

where  $c_{a0}$  is the initial number of active chains per unit volume (chain concentration, related to the mechanical properties of the material), and  $f_0(\mathbf{r})$  is the dimensionless distribution, such that  $\int f_0(\mathbf{r}) d\Omega = 1$ . The term *active chains* indicates the chains participating in the load bearing mechanism of the material, namely those connected at both ends to the neighboring chains, while dangling chains are not included in  $c_{a0}$ . The dimensionless distribution function is often assumed to be the standard Gaussian (normal distribution),  $f_0(|\mathbf{r}|) = \left(\frac{3}{2\pi N b^2}\right)^{\frac{3}{2}} \exp\left(-\frac{3|\mathbf{r}|^2}{2N b^2}\right)$ , with

mean value  $\mathbf{r} = 0$  and standard deviation  $b\sqrt{N/3}$  (Treloar, 1946). Since, according to the affine deformation hypothesis  $\mathbf{r} = |\mathbf{r}| = \lambda \mathbf{r}_0$ , (being  $\mathbf{r}_0 = b\sqrt{N}$  the average rest end-to-end vector length, while  $b$ ,  $\lambda$  are the Kuhn length and the current stretch of the chain, respectively), the dimensionless distribution function can be equivalently expressed as

$$f_0(\lambda) = \left(\frac{3}{2\pi N b^2}\right)^{\frac{3}{2}} \exp\left(-\frac{3\lambda^2}{2N b^2}\right) \text{ (Kuhn and Grün, 1942).}$$

According to be above observation, in a generic deformed state the chain distribution function  $f(\mathbf{r}, t)$  accounts for the active chains only, i.e. when some chains are lost (leading to a local damage of the material), the corresponding integral of the distribution function over the chains configuration space gives  $\int f(\mathbf{r}, t) d\Omega \leq 1$ . However, since the applied stress history could be responsible for non-isotropic damage, the distribution function loses its Gaussian character (see sect. 2.2) (Vernerey et al., 2017).

For brevity, we introduce the symbol  $\square = \int \square d\Omega = \int_0^{2\pi} \int_0^\pi \left( \int_0^{Nb} \square r^2 dr \right) \sin \theta d\theta d\omega$  representing the integration of the function of interest

$\square$  over the chain configuration space; it follows that  $c_a(t) = \langle \phi(\mathbf{r}, t) \rangle = c_{a0} \langle f(\mathbf{r}, t) \rangle$ , (Vernerey et al., 2017). According to the above described statistical approach, any mechanism responsible for the change of the chain distribution must be accounted for to determine the mechanical state of the material. The energy stored per unit volume of material  $\Psi$  can be evaluated by adding up all the contributions coming from the active chains, i.e. by integrating over the chain configuration space  $\Omega$  the energy of a single chain  $\psi(\mathbf{r})$  (usually assumed to be a function of  $\mathbf{r}$  only), weighted by the distribution function  $f$ , i.e.

$$\Psi = \int_{\Omega} \phi(\mathbf{r}, t) \psi(\mathbf{r}) d\Omega = c_{a0} \langle f(\mathbf{r}, t) \psi(\mathbf{r}) \rangle \quad (2)$$

$\rho(\mathbf{r}, t) = \phi(\mathbf{r}, t) \psi(\mathbf{r})$  being the energy density of the material in the current state.

The mechanical energy of the material in the undeformed state (in which  $\mathbf{F} = \mathbf{1}$ , being  $\mathbf{F}$  the deformation gradient tensor and  $\mathbf{1}$  the unit second order tensor) is nonzero, i.e.  $\Psi_0 = c_a f_0 \psi > 0$ , being the elastic

$$\dot{\phi}_V(\mathbf{r}, t) = c_a \dot{f}_V(\mathbf{r}, t), \text{ with } \dot{f}_V(\mathbf{r}, t) = k_a \frac{c_{max} - c_a}{c_a} f_0(\mathbf{r}) - k_d f(\mathbf{r}, t), \text{ or } \dot{\phi}_V(\mathbf{r}, t) = -k_d c_\mu (f(\mathbf{r}, t) - f_0(\mathbf{r})) \quad (6)$$

energy of a single chain equal to zero only when  $\mathbf{r} = 0$ . The potential energy per unit volume in the current (deformed) configuration is then provided by integrating the energy of a single chain times the difference of the dimensionless distribution functions (current and initial) over the chain configuration space, i.e.:

$$\Delta\Psi(t) = c_a \langle \Delta f(\mathbf{r}, t) \psi(\mathbf{r}) \rangle, \quad \Delta f(\mathbf{r}, t) = f(\mathbf{r}, t) - f_0(\mathbf{r}, 0) \quad (3)$$

A typical expression for  $\psi(\mathbf{r})$ , valid for both moderate and large deformations, is the one based on the Langevin function,  $\mathcal{L}(\square) = \coth(\square) - \square^{-1}$ , namely  $\psi(r) = Nk_B T \cdot \left( \frac{\beta}{bN} r + \ln \frac{\beta}{\sinh \beta} \right)$ , with  $\beta = \mathcal{L}^{-1}\left(\frac{r}{bN}\right) = \mathcal{L}^{-1}\left(\frac{i}{\sqrt{N}}\right)$ , where  $k_B$  and  $T$  are the Boltzmann constant and the absolute temperature, respectively (Treloar, 1946). The force existing in the chain can be obtained as  $\mathbf{t}(N) = \partial\psi(\lambda, N)/\partial\mathbf{r}$  (Gordon, 1975), where it has been emphasized the dependence of the chain force  $\mathbf{t}$  on the deformation  $\lambda$ , and on the number of Kuhn's segments  $N$  of the chains.

## 2.2. Micromechanical network model with internal remodeling

The time evolution of the distribution function  $\phi(\mathbf{r}, t)$  represents the key feature of the present micromechanical model; the time rate of the distribution function must account for the main involved mechanisms, namely the deformation and the strain-rate dependence,

$$\dot{\phi}(\mathbf{r}, t) = \dot{\phi}_L(\mathbf{r}, t) + \dot{\phi}_V(\mathbf{r}, t) \quad (4)$$

i.e. it has been expressed through the sum of the contribution of the deformation ( $\dot{\phi}_L$ , the subscript  $L$  indicates the dependence of the deformation rate on the velocity gradient  $\mathbf{L} = \dot{\mathbf{F}}\mathbf{F}^{-1}$ ) and of the strain-rate effects ( $\dot{\phi}_V$ ); in (4) the time can be considered a parameter associated to the evolution of the mechanical process and not necessarily as the physical time.

The contribution of the deformation is given by (Vernerey et al., 2017):

$$\dot{\phi}_L(\mathbf{r}, t) = -\phi_{,i} \dot{r}_{,i} - \phi \dot{r}_{i,i} = -(\phi_{,i} r_j + \phi \delta_{ij}) L_{ij} = -(\nabla\phi \otimes \mathbf{r} + \phi \mathbf{I}) : \mathbf{L} \quad (5)$$

where  $\dot{r}_i = L_{ij} r_j$  and  $\dot{r}_{i,i} = L_{ii}$ . It's worth noticing that for an incompressible material  $t\mathbf{r}\mathbf{L} = L_{ii} = 0$ , so Eq. (5) simplifies to  $\dot{\phi}_L = -\phi_{,i} r_j L_{ij}$  or, in tensorial form  $\dot{\phi}_L = -\operatorname{div}(\phi\mathbf{r})$ . The qualitative evolution of the distribution function upon stretching of the polymer's network is illustrated in Fig. 1 where a simple 2D chains distribution in the  $(r_x, r_y)$  space (being  $r_x = r_x/(bN)$ ,  $r_y = r_y/(bN)$ ) has been assumed for sake of clarity.

The second term in Eq. (4) accounts for the viscous response of the material. In the present model the time-dependence is described by the

internal microstructural rearrangement, mathematically expressed by (Vernerey et al., 2017):

where  $k_a, k_d$  are the chain bonds activation and deactivation frequencies, respectively.

In Eq. (6)  $c_\mu = c_a(t \rightarrow \infty) = \frac{k_a}{k_a + k_d} c_{max}$  is the steady state value of the chains concentration, related to the material's shear modulus  $\mu$  through the relation  $c_\mu = \frac{\mu}{k_B T}$ . Once the shear modulus is introduced in Eq. (6), only the deactivation rate  $k_d$  is relevant to the final expression of  $\dot{\phi}_V$ . For such a strain rate dependent mechanical model, the characteristic relaxation time is given by  $\tau = \frac{1}{k_d}$  (Vernerey et al., 2017; Vernerey, 2018).

Differently by classical approaches adopted to describe the viscoelastic response of materials often based on the Maxwell or the generalized Maxwell model (Shen et al., 2019), (Loew et al., 2019), the present time-dependent physics-based model is quite different being funded on the concept of internal remodeling of the material at the molecular scale. Within this approach no convolution integrals are needed and the strain history of the material does not require to be recorded during the load history but only the velocity gradient  $\mathbf{L}$  is needed. In analogy with the classical Maxwell model, the storage and loss modulus  $\mu^s$  and  $\mu^d$  can be defined; they are expressed through the deactivation rate  $k_d$  as follows (Lewandowski and Chorążczewski, 2010):

$$\mu^s = \mu \frac{k_d^{-2} \omega^2}{1 + k_d^{-2} \omega^2}, \quad \mu^d = \mu \frac{k_d \omega}{1 + k_d^{-2} \omega^2} \quad (7)$$

where  $\mu = c_\mu k_B T$  is the instantaneous shear modulus and  $\omega$  is the angular frequency of the oscillatory rheological test. The Maxwell model is typically used to model a viscoelastic fluid or a viscoplastic solid, and is consistent with the present micromechanical model based on the activation and deactivation of the chains of the network: the microstructure internal rearrangement entails the network to gradually approach a relaxed stress state under a fixed deformation (so the material does not recover its original shape after unloading), as occurs in a viscoelastic fluid.

Since the mechanical state of a polymer is related to its degree of cross-linking (quantified by the concentration  $c_a(t)$  of active chains) and to the statistical distribution of the chain end-to-end vectors  $f(\mathbf{r}, t)$ , the stress state in the material can be easily determined. The stress tensor is provided by the following derivative of the free energy with respect to the deformation gradient:

$$\mathbf{P}(t) = \frac{\partial \Delta\Psi(t)}{\partial \mathbf{F}} + J p(t) \mathbf{F}^{-T} \quad (8)$$

where  $\mathbf{P}$  is the (nominal) first Piola stress tensor, and  $p$  is the hydrostatic pressure, here introduced as a Lagrange multiplier to enforce the incompressibility condition assumed for the polymer (mathematically expressed by  $J = \det \mathbf{F} = 1$ ). By using (6), Eq. (8) becomes:

$$\mathbf{P}(t) = \frac{\partial \Delta\Psi(t)}{\partial t} \frac{\partial t}{\partial \mathbf{F}} = \frac{\partial \Delta\phi(\mathbf{r}, t) \psi(\mathbf{r})}{\partial t} \mathbf{F}^{-T} + J p(t) \mathbf{F}^{-T} = \dot{\phi} \psi \mathbf{F}^{-T} + p(t) J \mathbf{F}^{-T} = \langle [ -(\nabla\phi \otimes \mathbf{r}) : \mathbf{L} - k_d c_\mu (f - f_0) ] \psi \rangle \dot{\mathbf{F}}^{-T} + J p \mathbf{F}^{-T} \quad (9)$$

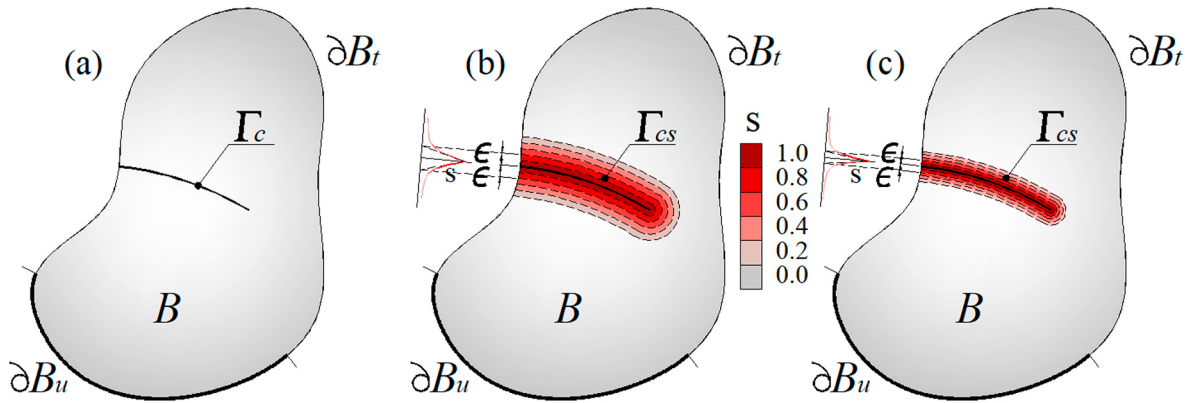


**Fig. 2.** Sharp crack  $\Gamma_c$  embedded in the solid  $\mathcal{B}$  (a) and its diffused representation  $\Gamma_{cs}$  through the phase-field variable  $s$  (b, c). As the phase-field length parameter  $\varepsilon$  tends to zero, the diffuse crack tends asymptotically to the sharp crack.

where the term  $1 : \mathbf{L} = \text{tr}\mathbf{L} = 0$  (see Eq. (5)) because of the incompressibility, while  $\dot{\mathbf{F}}^{-T} = \mathbf{L}^{-T}\mathbf{F}^{-T}$ . The divergence theorem applied to the first term in (9) (after assuming the boundary terms to vanish), leads to:

$$\begin{aligned} \langle [-(\nabla\phi \otimes \mathbf{r}) : \mathbf{L}] \psi \rangle &= \left[ \int_{\Omega} (\phi - \phi_0) [\nabla\psi(t) \otimes \mathbf{r}] d\Omega \right] \\ &: \mathbf{L} = \left[ \int_{\Omega} (\phi - \phi_0) \mathbf{t} \otimes \mathbf{r} d\Omega \right] : \mathbf{L} \end{aligned} \quad (10)$$

By referring to the actual deformed state, the (true) Cauchy stress tensor  $\boldsymbol{\sigma}$  can be obtained from the first Piola stress tensor through the following expression:

$$\boldsymbol{\sigma} = \mathbf{P}\mathbf{F}^T = \langle (\phi - \phi_0) \left[ \mathbf{t} \otimes \mathbf{r} - k_d \frac{c_u}{c_a} \psi \mathbf{L}^{-T} \right] \rangle + p1 \quad (11)$$

where the hydrostatic part  $p1$  of the stress tensor accounts for the incompressibility constraint.

The above presented micromechanical approach is suitable to be easily implemented into a finite element model; it can be adopted to determine the stress state at the Gauss point level – to be used for the evaluation of the corresponding nodal forces – required to determine the unbalanced nodal force vector of the iterative nonlinear solution process (see Sect. 4, Eqs 20–22).

### 3. Phase-field modeling of fracture

The so-called regularized approach to fracture, typically consists in introducing an approximate smooth description of the actual physical discontinuity, whose discrete character is recovered only when the length parameter  $\varepsilon$  vanishes. Let us assume that the body in its undeformed configuration occupies the region  $\mathcal{B}_0 \subset \mathbb{R}^d$ ,  $d$  being the dimension of the space ( $d = 1, 2, 3$ ), while  $\partial\mathcal{B}_0$  represents the boundary of  $\mathcal{B}_0$ . The body is assumed to contain a sharp discontinuity  $\Gamma_{c0} \subset \mathbb{R}^{d-1}$  that in fracture mechanics represents the crack. Being the polymeric materials prone to large deformations, we correspondingly introduce the deformed counterpart of the solid domain, i.e. we assume that the deformed body occupies the region  $\mathcal{B} \subset \mathbb{R}^d$ , bounded by  $\partial\mathcal{B}$ , while the corresponding sharp discontinuity is now indicated as  $\Gamma_c \subset \mathbb{R}^{d-1}$ .

An auxiliary field variable (also known as order parameter or, simply, phase-field)  $s(\mathbf{x}, t)$ , that assuming values in the interval  $0 < s \leq 1$ , quantifies in a diffuse way the discontinuity existing in the material: it takes the value  $s = 0$  in the solid (or undamaged) material while it becomes  $s = 1$  in the cracked (fully damaged) one. Intermediate values, occurring in a region close to the crack, indicate the transition between the failed ( $s \rightarrow 1^-$ ) and the unfailed ( $s \rightarrow 0^+$ ) material. According to the

definitions above, the crack is provided by the one level set of  $s(\mathbf{x}, t)$ . This way of representing a real sharp interface, spreads the crack in a narrow region  $\Gamma_{cs} \subset \mathbb{R}^d$  that tends asymptotically to the real crack as the scale parameter vanishes, i.e. when  $\varepsilon \rightarrow 0$  (Fig. 2).

The solution of the fracture problem can be conveniently expressed through the minimization of the following energy functional:

$$\Pi = \Psi_b + \Psi_s = \int_{\mathcal{B}} \Delta\Psi(\mathbf{r}, t) dV + G_c \int_{\Gamma_c} dA \quad (12_1)$$

$$\text{where } \Psi_s = G_c \int_{\Gamma_c} dA = G_c \int_{\mathcal{B}} \gamma(s, \nabla s) dV \quad (12_2)$$

i.e., according to the variational theory of fracture (Francfort and Marigo, 1998), the crack growths by following a path that ensures that the total energy (12<sub>1</sub>) of the system is minimized. The second term in (12<sub>2</sub>) accounts for the surface fracture energy, where  $G_c$  is the fracture energy per unit cracked area, while  $\Gamma_c$  is the current crack domain, and  $\gamma(s, \nabla s)$  is the crack surface density function representing the actual fracture domain  $\Gamma_c$  through the continuous function  $\gamma$ , i.e.  $\Gamma_c = \int_{\mathcal{B}} \gamma(s, \nabla s) dV$ .

The phase-field function  $s(\mathbf{x}, t)$  can be derived from the solution of the differential equation  $s - \varepsilon^2 \Delta s = 0$  with b.c.  $\nabla s \cdot \mathbf{n} = 0$  on  $\partial\mathcal{B}$  ( $\Delta$ ,  $\nabla$  being the Laplacian and the gradient operator, respectively, while  $\mathbf{n}$  is the unit outward normal to the boundary  $\partial\mathcal{B}$  of  $\mathcal{B}$ ) (Miehe et al., 2010a) or, equivalently, from the condition of minimum of a functional usually assumed as crack surface density function:

$$I(s) = \int_{\mathcal{B}} \gamma(s, \nabla s) dV = \frac{1}{2\varepsilon} \int_{\mathcal{B}} s^2 + \varepsilon^2 |\nabla s|^2 dV \quad (13)$$

The energy functional of the problem (see Eq. (12<sub>1</sub>)) can thus be redefined as follows:

$$\Pi = \Psi_b + \Psi_s = \int_{\mathcal{B}} g(s) \Delta\Psi(\mathbf{r}, t) dV + \frac{G_c}{2\varepsilon} \int_{\mathcal{B}} s^2 + \varepsilon^2 |\nabla s|^2 dV \quad (14)$$

being  $g(s)$  the stress degradation function, quantifying the stiffness loss for a partially damaged material, usually expressed as  $g(s) = [(1-s)^2 + \eta]$  (Miehe et al., 2010b), being  $\eta$  a small number providing some material's residual stiffness required for computational stability reasons (Borden et al., 2012).

In a similar way, the stress tensor field (11) must account for the diffuse crack, i.e. it has to relax in the damaged material; it has to be corrected exactly as we did for the bulk energy (Bhowmick and Liu, 2018b), i.e.

$$\tilde{\sigma} = [(1-s)^2 + \eta] \cdot \left[ \left\langle (\phi - \phi_0) \left[ \mathbf{t} \otimes \mathbf{r} - k_d \frac{c_\mu}{c_a} \psi \mathbf{L}^{-T} \right] \right\rangle + p_1 \right] \quad (15)$$

The above expression for the stress tensor can be derived from the variation of the functional (14), as shown in the following.

#### 4. Phase-field in the large deformation regime of rate-dependent polymers: numerical implementation

The above-stated variational problem can be solved for the field variables  $\mathbf{u}, s$  through the stationarity condition of the total energy of system (14); since we are considering the case of large deformation, the variational approach will be hereafter written in the reference configuration  $\mathcal{B}_0$ . The first variation of the functional, written by including the potential of the external forces  $\Psi_e$ , is expressed by:

$$\delta_{\mathbf{u}, s}(\Pi + \Psi_e) = \frac{\partial(\Pi + \Psi_e)}{\partial \nabla \mathbf{u}} \delta \mathbf{u} + \frac{\partial(\Pi + \Psi_e)}{\partial s} \delta s = - \int_{\mathcal{B}_0} \left( [(1-s)^2 + \eta] \operatorname{Div} \mathbf{P} + \mathbf{B} \right) \delta \mathbf{u} dV + \int_{\mathcal{B}_0} \left[ 2(s-1) \Delta \Psi + G_c \left( \frac{s}{\varepsilon} - \varepsilon \Delta s \right) \right] \delta s dV + \int_{\partial \mathcal{B}_0} \left( [(1-s)^2 + \eta] \mathbf{P} n - \bar{\mathbf{T}} \right) \delta \mathbf{u} dA + \int_{\partial \mathcal{B}_0} \nabla s \cdot n \delta s dA = 0 \quad (16)$$

being  $\mathbf{B}$ ,  $\bar{\mathbf{T}}$ ,  $n$  the body force, the traction force and the normal vector, respectively, referred to the material (undeformed) configuration of the body occupying the domain  $\mathcal{B}_0$  with boundary  $\partial \mathcal{B}_0 = \partial \mathcal{B}_{0u} \cup \partial \mathcal{B}_{0T}$ . By localizing the above stationarity condition, the final governing equations with the corresponding boundary conditions, can be finally obtained:

$$\begin{aligned} & [(1-s)^2 + \eta] \operatorname{Div} \mathbf{P} + \mathbf{B} = 0 \quad \text{in } \mathcal{B}_0 \\ & 2(s-1) \Delta \Psi + G_c \left( \frac{s}{\varepsilon} - \varepsilon \Delta s \right) = 0 \quad \text{in } \mathcal{B}_0 \\ & \mathbf{u} = \bar{\mathbf{u}} \quad \text{in } \partial \mathcal{B}_{0u} \\ & [(1-s)^2 + \eta] \mathbf{F} \mathbf{S} n = \bar{\mathbf{T}} \quad \text{in } \partial \mathcal{B}_{0T} \\ & \nabla s \cdot n = 0 \quad \text{in } \partial \mathcal{B}_0 \end{aligned} \quad (17)$$

They represent a system of coupled equations consisting of the balance of linear momentum and the phase-field evolution equation, equipped with the standard essential and natural and boundary conditions for the stress field as well as for the phase-field, namely  $\nabla s \cdot n = 0$  that is associated to (17)<sub>2</sub>. When a generic load history is considered, in order to motivate the diffusive character of the phase-field evolution, in the above expression the density energy term  $\Delta \Psi$  must account for the energy history occurred in the material, so a history field parameter must be defined as  $\mathcal{H} := \max_{t \in [0, t_f]} \Delta \Psi(\mathbf{X}, t)$  (Miehe and Schänzel, 2014), being  $t_f$  the current time instant. In order to properly describe the response of a material undergoing fracture under tensile stress, a tensile-compression split of the phase-field driving force has to be considered in order to prevent cracking under compressive stress states, i.e. a tensile-compression decomposition of the deformation energy  $\Delta \Psi$  has to be considered (Teichtmeister et al., 2016), (Miehe and Schänzel, 2014).

For computational purpose, the above equations can be discretized by introducing the standard finite element discretization of the involved fields (displacements, deformation, phase-field and phase-field gradient), i.e.:

$$\begin{aligned} \bar{\mathbf{u}} &= \sum_{i=1}^{n_n} [\mathbf{N}]_i \mathbf{u}_i, & \bar{\mathbf{F}} &= + \sum_{i=1}^{n_n} [\mathbf{B}_u]_i \mathbf{u}_i, \\ \bar{s} &= \sum_{i=1}^{n_n} N_i s_i, & \bar{\nabla} s &= \sum_{i=1}^{n_n} [\mathbf{B}_s]_i s_i \end{aligned} \quad (18)$$

where the upper bar terms are the element's interpolated vector or scalar quantities,  $n_n$  represents the number of nodes of the element,  $\mathbf{u}_i, s_i$  are the nodal displacements and the nodal values of the phase-field parameter, respectively,  $N_i$  denotes the shape function associated to the  $i$ -th node, while the matrices in (18) are:

$$\begin{aligned} [\mathbf{N}]_i &= \begin{bmatrix} N_i & 0 \\ 0 & N_i \end{bmatrix}, & [\mathbf{B}_u]_i &= \begin{bmatrix} N_{i,X} & 0 & N_{i,Y} & 0 \\ 0 & N_{i,Y} & 0 & N_{i,X} \end{bmatrix}^T, \\ & & &= \begin{bmatrix} 1 & 0 \\ 0 & 1 \end{bmatrix}, & [\mathbf{B}_s]_i &= [N_{i,X} \quad N_{i,Y}]^T \end{aligned} \quad (19)$$

In order to provide the irreversible character of the phase-field evolution (Miehe et al., 2010a), at any time it must be  $\dot{s} \geq 0$ , so if it happens that  $\delta \mathcal{H} / \delta s > 0$ , the time derivative of the phase-field variable has to be set to zero,  $\dot{s} = 0$ . The equations corresponding to the equi-

librium and phase-field evolution can be expressed via the following residuals:

$$\begin{aligned} \mathbf{R}_u &= \int_{\mathcal{B}_0} \left[ (1-s)^2 + \eta \right] \nabla \mathbf{S} dV - \left( \int_{\mathcal{B}_0} \mathbf{B} dV + \int_{\partial \mathcal{B}_0} \bar{\mathbf{T}} dA \right) \\ R_s &= \int_{\mathcal{B}_0} \dot{s} M + G_c \left( \frac{s}{\varepsilon} + \varepsilon \nabla^2 s \right) dV + \int_{\mathcal{B}_0} 2(s-1) \Delta \Psi dV \end{aligned} \quad (20)$$

or, in the discretized form, by referring to the  $i$ -th degree of freedom:

$$\begin{aligned} R_{ui} &= \int_{\mathcal{B}_0} \left[ (1-N_i s_i)^2 + \eta \right] [\mathbf{B}_u]_i^T \mathbf{P} dV - \left( \int_{\mathcal{B}_0} N_i^T \mathbf{B} dV + \int_{\partial \mathcal{B}_0} N_i^T \bar{\mathbf{T}} dA \right) \\ R_s &= \int_{\mathcal{B}_0} G_c \varepsilon [\mathbf{B}_s]_i^T \nabla s + \left( \frac{G_c}{\varepsilon} + 2N_j \Delta \Psi_j \right) N_i s_i dV - \int_{\mathcal{B}_0} 2N_j \Delta \Psi_j dV \end{aligned} \quad (21)$$

Upon linearization, in incremental form the above nonlinear problem reads

$$\mathbf{K}_T \left\{ \begin{array}{l} \Delta \mathbf{u} \\ \Delta s \end{array} \right\} = - \left\{ \begin{array}{l} \mathbf{R}_u \\ R_s \end{array} \right\} \quad (22)$$

being  $\mathbf{R}_u, R_s$  the mechanical and phase-field residual vectors, while  $\mathbf{K}_T$  is the tangent matrix of the coupled problems, explicitly written as:

$$\mathbf{K}_T = \mathbb{A}_{e=1}^{ne} \mathbf{K}_T^e = \mathbb{A}_{e=1}^{ne} \begin{bmatrix} \mathbf{K}_{Tuu}^e & \mathbf{K}_{Tus}^e \\ \mathbf{K}_{Tsu}^e & \mathbf{K}_{Tss}^e \end{bmatrix} \quad (23a)$$

$$\mathbf{K}_{Tuu}^e = \frac{\partial \mathbf{R}_u^e}{\partial \mathbf{u}} = \int_{\Omega_{0e}} \left[ (1-N_i s_i)^2 + \eta \right] \mathbf{B}_u^T \frac{\partial^2 \Delta \Psi}{\partial \mathbf{E}^2} \mathbf{B}_u d\Omega \quad (23b)$$

$$\mathbf{K}_{Tus}^e = \frac{\partial \mathbf{R}_u^e}{\partial s} = \int_{\Omega_{0e}} -2(1-N_i s_i) \mathbf{B}_u^T \mathbf{P} \mathbf{N}_s d\Omega \quad (23c)$$

$$\mathbf{K}_{Tsu}^e = \frac{\partial \mathbf{R}_s^e}{\partial \mathbf{u}} = \int_{\Omega_{0e}} -2(1-N_i s_i) \mathbf{N}_s^T \mathbf{P}^T \mathbf{B}_u d\Omega \quad (23d)$$

$$\mathbf{K}_{Tss}^e = \frac{\partial \mathbf{R}_s^e}{\partial s} = \int_{\Omega_{0e}} G_c \varepsilon \mathbf{B}_s^T \mathbf{B}_s + \mathbf{N}_s^T \left( \frac{G_c}{\varepsilon} + 2\Delta \Psi_m \right) \mathbf{N}_s d\Omega \quad (23e)$$

In (23a)  $\mathbb{A}$  indicates the assembly operator,  $\mathbf{K}_T^e$  is the tangent stiffness

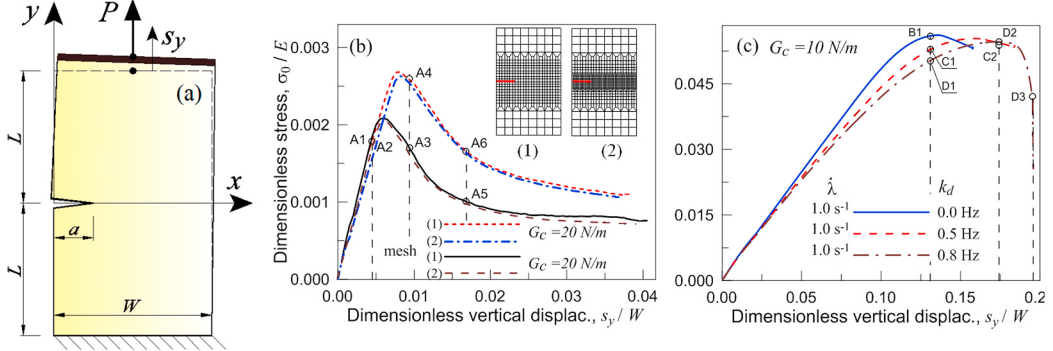


**Fig. 3.** (a) Cracked plate under a tensile force  $P$ . (b) Dimensionless stress vs dimensionless displacement for the elastic plate and (c) for the polymeric one; three values of the dynamic bond detachment frequency have been considered:  $k_d = 0 \text{ Hz}$ ,  $k_d = 0.5 \text{ Hz}$ ,  $k_d = 0.8 \text{ Hz}$ .

matrix of the element  $e$  (obtained by properly arranging the tangent sub-matrices  $\mathbf{K}_{Tuu}^e$ ,  $\mathbf{K}_{Tus}^e$ ,  $\mathbf{K}_{Ts}^e$  and  $\mathbf{K}_{Tss}^e$ ),  $\mathbf{C} = \partial^2 \Delta\Psi / \partial\mathbf{E}^2$  is the fourth-order tangent elastic tensor of the material,  $\mathbf{E} = \frac{1}{2}(\mathbf{F}^T \mathbf{F} - \mathbf{I})$  is the Green-Lagrange deformation tensor,  $\Omega_{0e}$  is the domain of the undeformed finite element  $e$ , and  $\mathbf{N}_s$  is the matrix collecting the standard shape functions  $N_i$  related to the generic node  $i$  of the element (the functions  $N_i$  must be properly arranged in  $\mathbf{N}_s$  for the interpolation of the phase-field variable within the element).

It is worth noticing that, in the case the body contains a pre-existing crack, from the computational viewpoint it can be modeled as a real physical crack (through a proper domain discretization) or it can be represented by setting the phase-field variable accordingly, and by setting an initial strain-history energy field in the form (Borden et al., 2012):

$$\Delta\Psi_m(\mathbf{X}, t=0) = c \begin{cases} \frac{G_c}{2\varepsilon} \left(1 - \frac{d_{\Gamma_c}(\mathbf{X})}{\varepsilon}\right) & \text{if } d_{\Gamma_c}(\mathbf{X}) \leq \varepsilon \\ 0 & \text{if } d_{\Gamma_c}(\mathbf{X}) > \varepsilon \end{cases} \quad (24)$$

being  $d_{\Gamma_c}(\mathbf{X})$  the distance of the point  $\mathbf{X}$  from the crack line  $\Gamma_c$  and  $c$  is a constant; if  $d_{\Gamma_c}(\mathbf{X}) \leq \varepsilon$  the energy is set equal to the surface crack energy, while it decays to zero within the small distance  $\varepsilon$ . The strategy based on physically modeling the pre-existing crack has been adopted in the following.

The above presented FE computational procedure has been implemented in a in-house code by using an updated Lagrangian approach within a staggered solution scheme, and a tensile-compression decomposition of the deformation energy  $\Delta\Psi$  of the material is adopted; nodal displacements and pressure values are assumed as unknowns. The developed computational framework enables to solve the mechanical

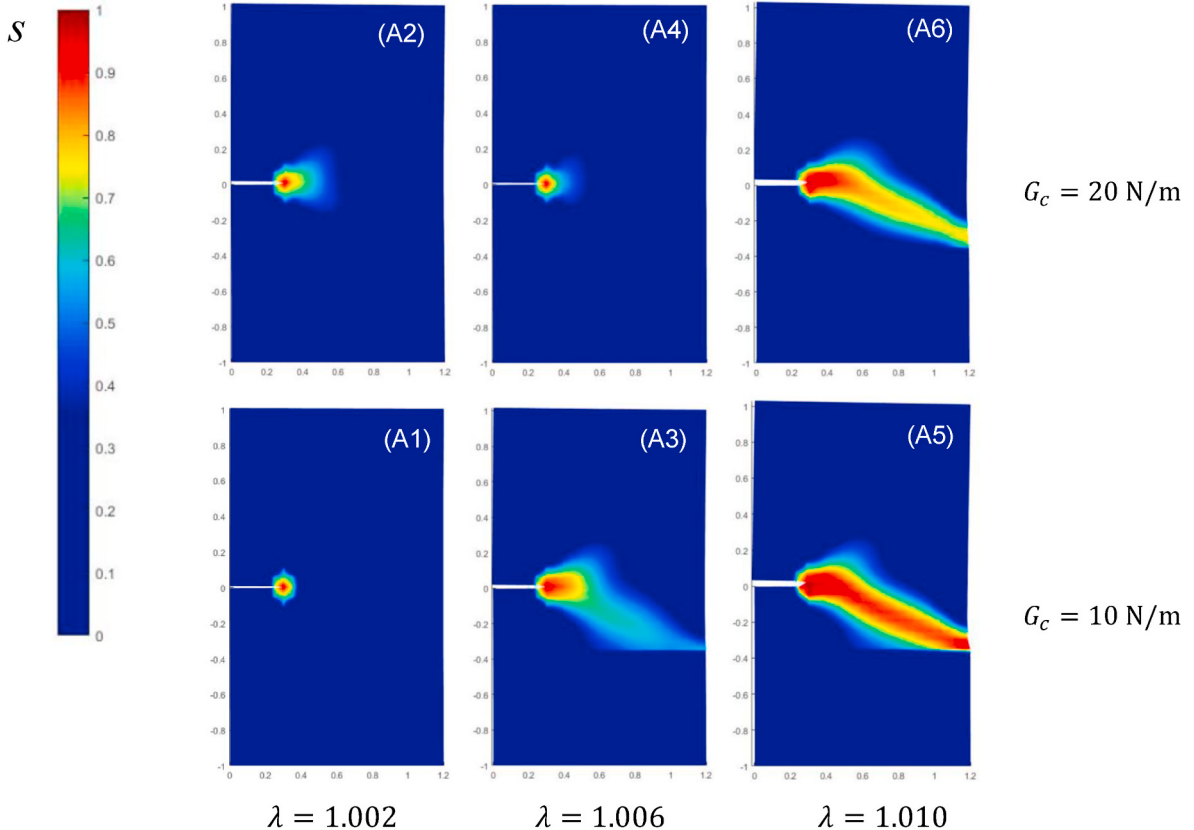


**Fig. 4.** Crack patterns corresponding to the states (A1, A2, A3, A4, A5, A6) indicated in Fig. 3b, obtained from the phase field approach for the elastic plate.

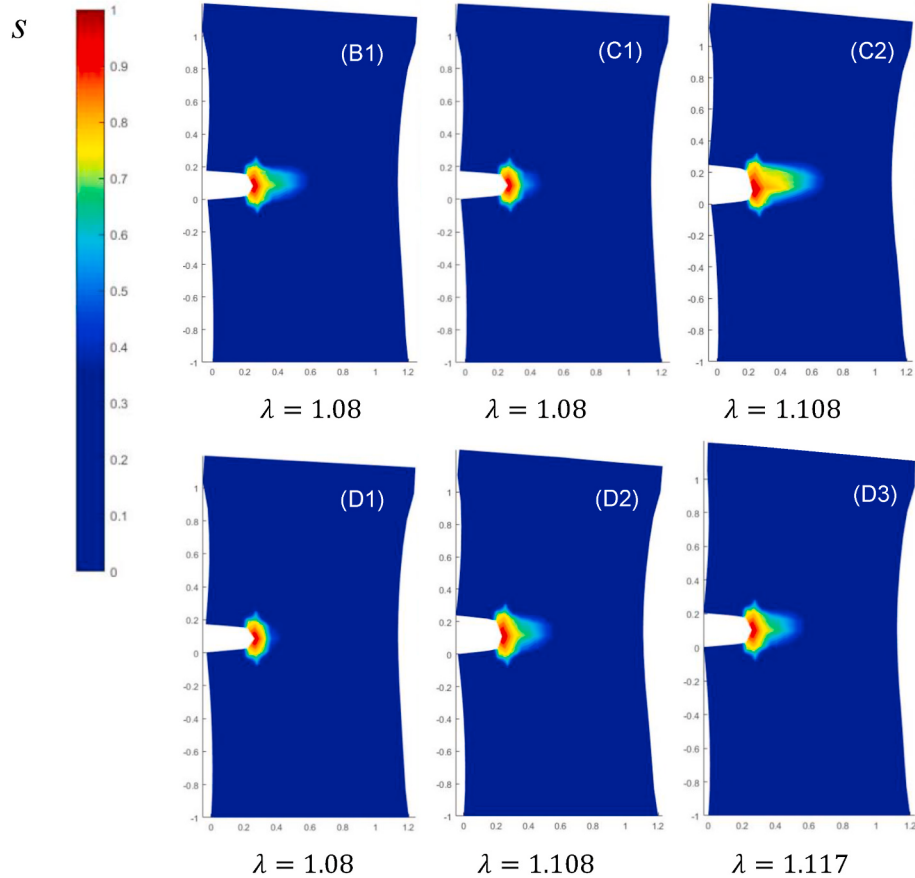


**Fig. 5.** Crack patterns corresponding to the states indicated in Fig. 3c, obtained from the phase field approach for the rubber plates with different dynamic bond parameter  $k_d$  (B1,  $k_d = 0$ ; C1, C2,  $k_d = 0.5$  Hz; D1, D2, D3,  $k_d = 0.8$  Hz).

and the phase field evolution problems alternatively, by assuming a reasonable small time integration step throughout the analysis (Hofacker and Miehe, 2012).

## 5. Numerical examples

In the present section some parametric examples involving 2D pre-cracked elements made of elastic or viscoelastic polymeric materials are considered. The above described computational approach has been implemented in a in-house FE code, while the analyses have been

performed by adopting a sufficiently small time step (0.5–1.0 ms), while the convergence of the solution has been evaluated on the basis of suitable tolerances (expressed in terms of both unbalanced forces and incremental displacements) of about 0.2%. The phase field solution has typically shown to converge within 3–4 iterations.

### 5.1. Edge cracked plate under a tensile point load

The first example considers the fracture of an edge cracked plate under tension: a rectangular plate with dimensions  $W \times 2L \times$

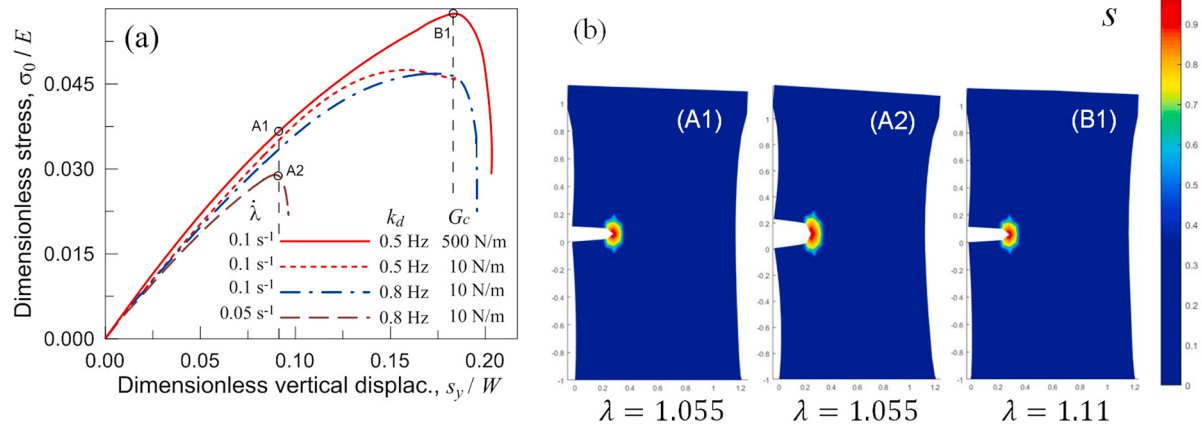


**Fig. 6.** (a) Dimensionless load vs dimensionless displacement for the elastomeric plate for different deformation rates and fracture energy values. Phase field maps corresponding to the point indicated in (a) (A1, B1,  $k_d = 0.5$  Hz; A2,  $k_d = 0.8$  Hz).

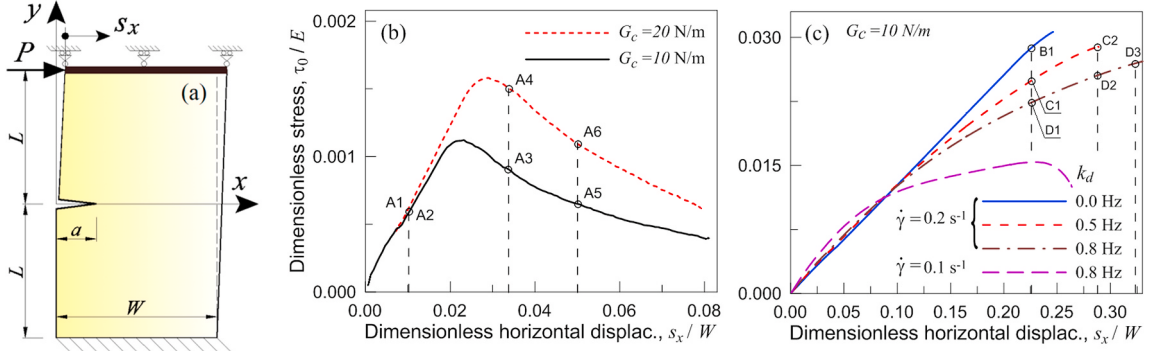


**Fig. 7.** (a) Cracked plate under a shear force  $P$ . (b) Dimensionless shear stress vs dimensionless displacement for the elastic plate and (c) for the polymeric one; three values of the dynamic bond detachment frequency have been considered:  $k_d = 0 \text{ Hz}$ ,  $k_d = 0.5 \text{ Hz}$ ,  $k_d = 0.8 \text{ Hz}$ .

$t$ (thickness) is restrained at its bottom edge and is loaded through a rigid element by a force  $P$  applied to the upper edge's midpoint (Fig. 3). The plate contains an initial straight edge crack having length  $a/W = 0.3$ , whereas the geometrical ratios of the plate are  $L/W = 1.2$  and  $t/W = 0.1$ . The material is assumed to be in plane stress and has the following mechanical properties: elastic modulus  $E = 20 \text{ MPa}$ , Poisson's ratio  $\nu = 0.495$ . Firstly, the case of an elastic material is examined (fracture energy  $G_c = 10 \text{ N/m}$  and  $G_c = 20 \text{ N/m}$ ) as well as the case of a polymeric plate with the same mechanical properties. Moreover, the polymeric material is assumed to be strain rate-dependent, whose severity is quantified by different deactivation frequencies (see sect. 2.2), i.e.  $k_d = 0 \text{ Hz}$  (no rate dependence),  $k_d = 0.5 \text{ Hz}$  and  $k_d = 0.8 \text{ Hz}$ ; the macroscopic stretch rate applied to the plate has been assumed to be equal to  $\dot{\lambda} = 1.0 \text{ s}^{-1}$  for all cases except when a different value is specified. The phase field calculation has been performed by adopting the length

parameter equal to  $\varepsilon/W = 0.05$ . In the present examples, we adopt a highly deformable material that is typically defect tolerant and for which the crack development takes place as a narrow damaged region that does not require to be described by using a very small length scale parameter. It has been shown that the phase-field approach is nearly mesh independent (being the fracture energy consistency intrinsic in the phase field formulation, (Miehe et al., 2010a)), while the length scale can be chosen as a numerical parameter whose value does not heavily influences the results, if assumed small enough compared with the problem dimensions (Mandal et al., 2019), (Wu and Nguyen, 2018).

In order to ensure a proper representation of the phase field in the computational approach, in the region where the crack is expected to develop, the size of the adopted finite elements has been assumed to be less than  $\varepsilon/2$ , enabling a reasonable resolution of the non-uniform damage field developing in the material. In Fig. 3a the geometry and

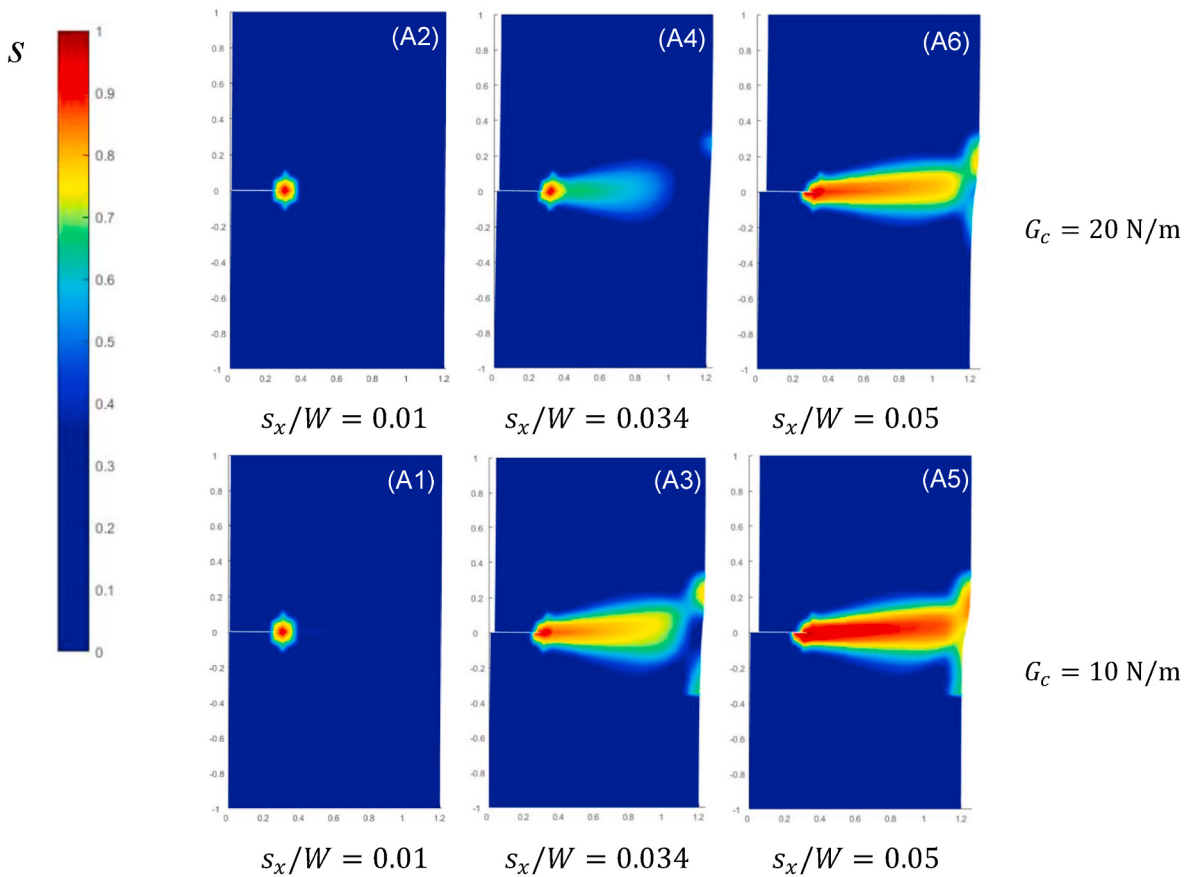


**Fig. 8.** Crack patterns corresponding to the states (A1, A2, A3, A4, A5, A6) indicated in Fig. 7b, obtained from the phase field approach for the elastic plate.

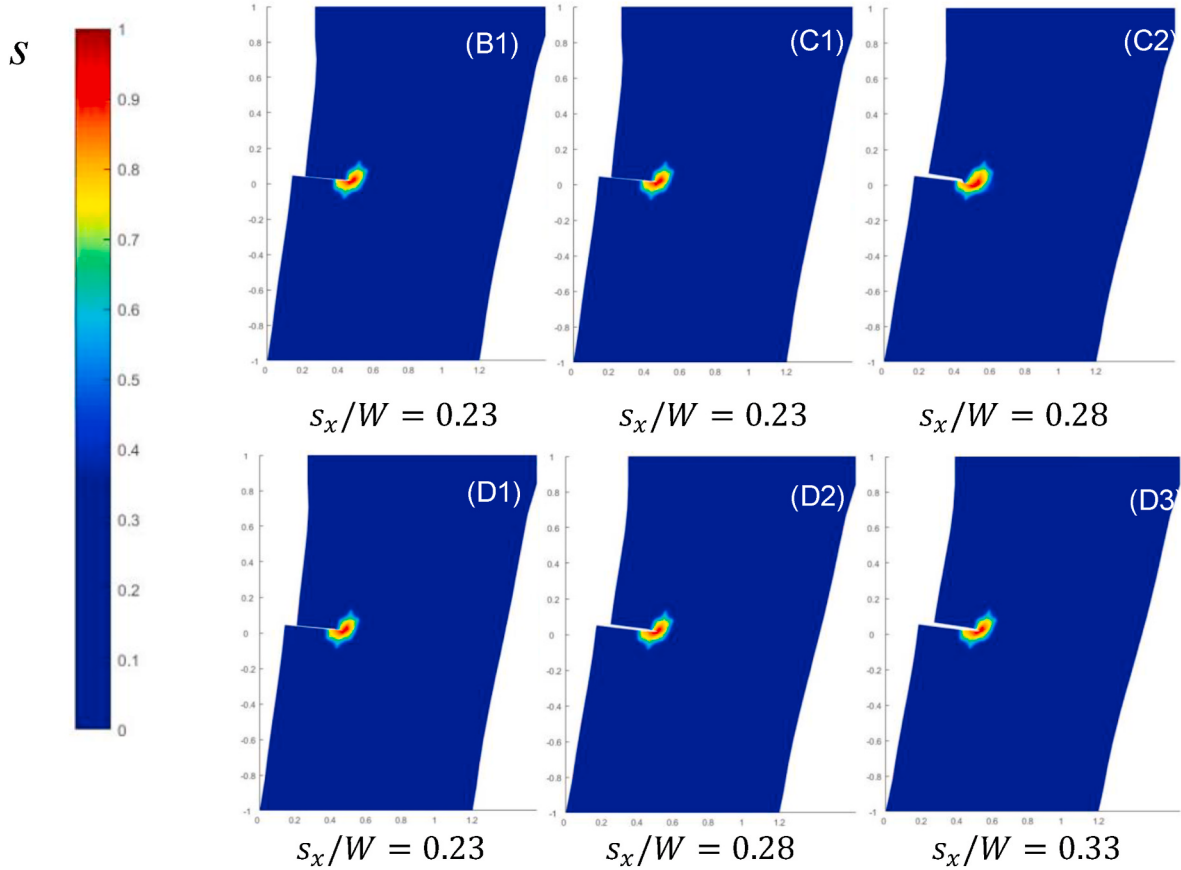


**Fig. 9.** Crack patterns corresponding to the states indicated in Fig. 7c, obtained from the phase field approach for the rubber plates with different dynamic bond parameter  $k_d$  (B1,  $k_d = 0$ ; C1, C2,  $k_d = 0.5 \text{ Hz}$ ; D1, D2, D3,  $k_d = 0.8 \text{ Hz}$ ).

the qualitative deformed shape of the plate are shown, while Fig. 3b and c displays the dimensionless remote nominal stress vs dimensionless displacement (the dimensionless nominal stress is defined as  $\sigma_0 = P/(W \times t)$ , while the dimensionless displacement is provided by  $s_y/W$ ); the analysis related to the elastic material has been performed by adopting two different meshes (see insert of Fig. 3b) in order to verify the robustness of the developed computational approach. It can be appreciated that the elastic plate presents a more brittle response, while the rubber ones are more prone to withstand the crack without failure, so the peak load as well as the maximum displacement reached are much greater than in the case of the purely elastic material.

Moreover, the viscoelastic character of the polymeric material, quantified by the deactivation parameter  $k_d$  (see sect. 2.2), entails a stress relaxation in the material allowing the plate to better tolerate the presence of the crack, leading to a response practically without any crack growth.

Fig. 4 shows the crack pattern developed in the elastic plate at different steps of the loading process (see Fig. 3b), while Fig. 5 displays the crack development in the elastomeric plate for different values of the deactivation rates  $k_d$  (Fig. 3c). The crack paths arising in the elastic material is much more pronounced than the ones appearing in the elastomeric plate; furthermore, because of the non-symmetric character of the load applied to the cracked plate, the crack develops following a downward bended path. It appears that the polymeric plate is much less prone to develop crack growth because of the lower stress values arising close to the crack tip. Furthermore, the more the relaxation the less the crack development, indicating that the viscoelastic behavior enhances the defect tolerance of the material. Finally, it is worth noticing that the phase field map represents a narrow damaged region rather than a sharp crack, because of the highly deformable character of the material

adopted for the plate.

In order to clearly outline the role of the viscoelastic response, in the following we consider the case with  $k_d = 0.8 \text{ Hz}$  but under a slower deformation rate, i.e.  $\dot{\lambda} = 0.5 \text{ s}^{-1}$ ; for such a case Fig. 6 shows the dimensionless load vs dimensionless displacement curves, compared to the case with  $\dot{\lambda} = 1.0 \text{ s}^{-1}$ . The lower deformation rate allows the material to relax more easily, leading to the failure of the plate not because of the crack growth but due to the remarkable stress loss. Because of the lower deformation rate, the material is allowed to easily reset the configuration state of its chains (see Eq. (6)), as provided by the increase of the time rate  $\dot{f}_V = -k_d c_\mu [f(\mathbf{r}, t) - f_0(\mathbf{r})]$ , indicating that the equilibrium is more close to the initial stress-free distribution,  $f_0$ , rather than the current one corresponding to the deformed material,  $f(\mathbf{r}, t)$ . As a consequence, the crack development is practically absent when the deformation rate is sufficiently small. In the same figure, the case of a viscoelastic polymer with  $k_d = 0.5 \text{ Hz}$ , loaded at  $\dot{\lambda} = 1.0 \text{ s}^{-1}$  and with  $G_c = 500 \text{ N/m}$  is also reported for sake of comparison; in this latter case the crack does not develop at all because of the very high fracture energy, so the response is only governed by the viscoelastic behavior.

## 5.2. Edge cracked plate under shear load

The same plate considered in the previous section is herein studied in the case of a shear load. The geometrical as well as the mechanical characteristics of the cracked plate are the same as those considered above (the mesh (2) is adopted, Fig. 3b). The case of the polymeric plate is solved by considering different viscoelastic properties, i.e. three network chains deactivation frequencies are assumed, namely  $k_d = 0 \text{ Hz}$  (no rate-dependence),  $k_d = 0.5 \text{ Hz}$  and  $k_d = 0.8 \text{ Hz}$ , while the macroscopic shear rate applied to the plate has been assumed to be equal to  $\dot{\gamma} =$

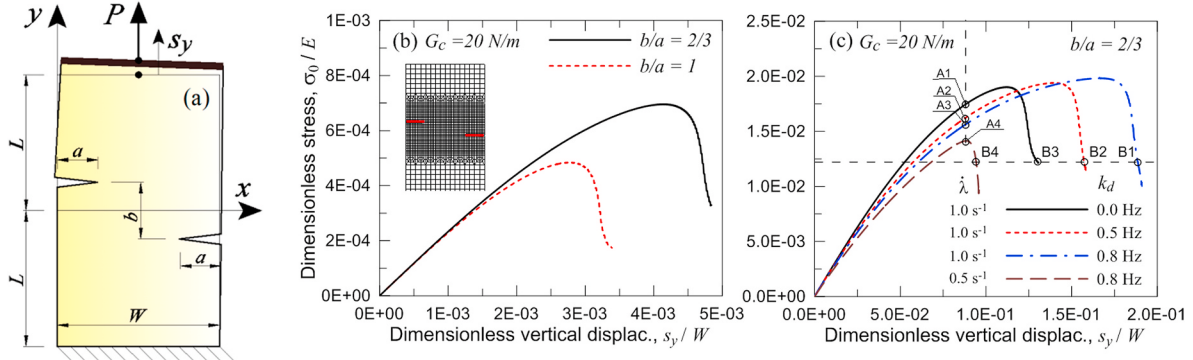


**Fig. 10.** (a) Cracked plate under a shear force  $P$ . (b) Dimensionless shear stress vs dimensionless displacement for the adopted FE discretization) and (c) for the viscoelastic polymeric one; three values of the dynamic bond detachment frequency have been considered:  $k_d = 0 \text{ Hz}$ ,  $k_d = 0.5 \text{ Hz}$ ,  $k_d = 0.8 \text{ Hz}$ .

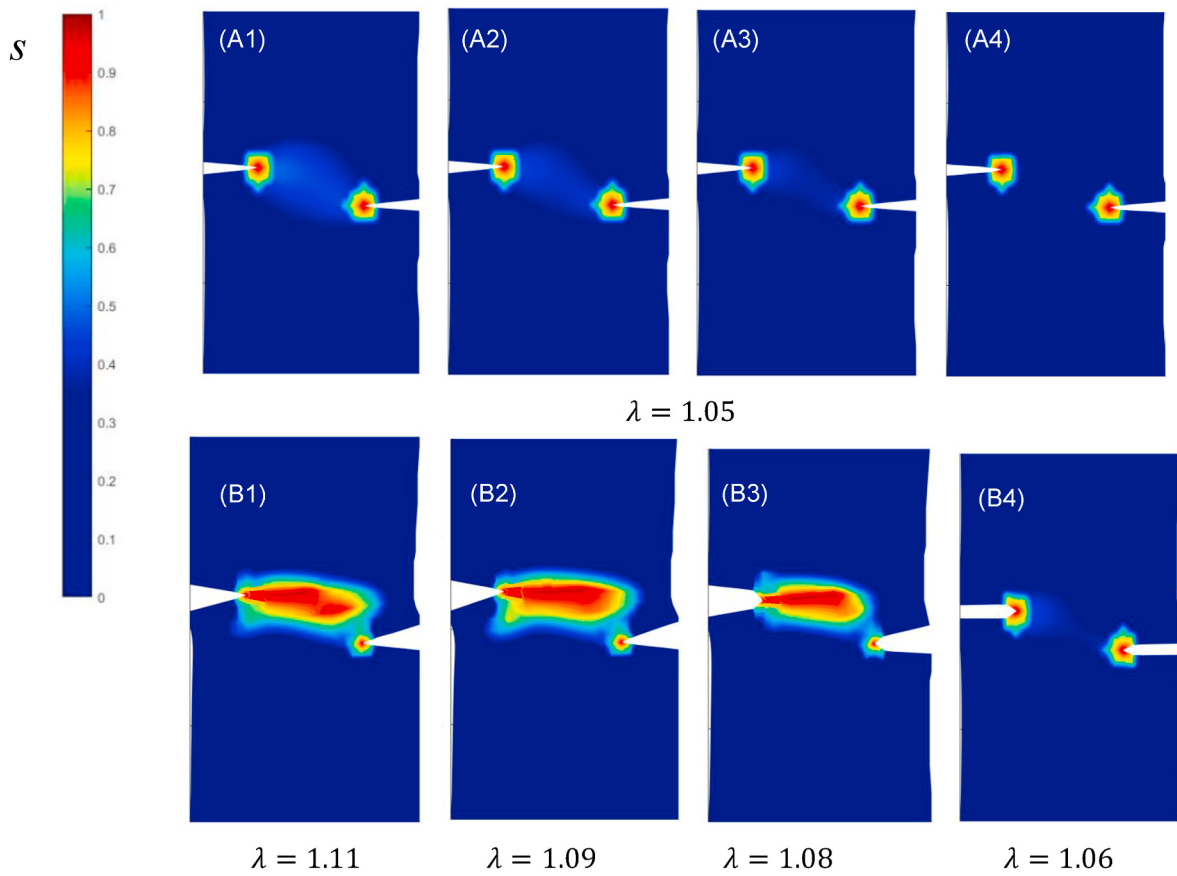


**Fig. 11.** (a) Dimensionless load vs dimensionless displacement for the elastomeric plate stretched at the deformation rate  $\dot{\lambda} = 1.0 \text{ s}^{-1}$  first 3 columns from left) and at  $\dot{\lambda} = 0.5 \text{ s}^{-1}$  (last column on the right). The maps of the phase field correspond to the points indicated in Fig. 10c (A1,  $k_d = 0 \text{ Hz}$ ; A2,  $k_d = 0.5 \text{ Hz}$ ; A3,  $k_d = 0.8 \text{ Hz}$ ; A4,  $k_d = 0.8 \text{ Hz}$ , B1,  $k_d = 0 \text{ Hz}$ ; B2,  $k_d = 0.5 \text{ Hz}$ ; B3,  $k_d = 0.8 \text{ Hz}$ ; B4,  $k_d = 0.8 \text{ Hz}$ ).

$0.5 \text{ s}^{-1}$ ; the case characterized by the greatest  $k_d$  value has also been studied under a slower shear rate, namely  $\dot{\gamma} = 0.25 \text{ s}^{-1}$ . Fig. 7a illustrates the geometry and the qualitative deformed shape of the plate under shear, while Fig. 7b and c provide the dimensionless remote nominal shear stress vs the dimensionless horizontal displacement of the top edge of the plate (dimensionless nominal shear stress evaluated as  $\tau_0 = P/(W \times t)$ , dimensionless displacement  $s_x/W$ ). The elastic plates responds in a more brittle fashion compared to the polymeric ones, with a softening post-peak branch; however, the plate made of viscoelastic polymeric material does not show any evident peak load and reaches high values of the horizontal displacements without failing, indicating a

more ductile behavior. Higher values of the viscoelastic-related parameter  $k_d$  corresponds to a softer response, indicating that the material undergoes a more pronounced stress relaxation in time, responsible for preventing the crack to grow.

The case of a viscoelastic material with  $k_d = 0.8 \text{ Hz}$  and slower shear rate ( $\dot{\gamma} = 0.25 \text{ s}^{-1}$ ) is also shown in Fig. 7c; a quite different response can be appreciated because of the high stress relaxation, allowed by the lower deformation rate, taking place in the material. In Fig. 8, the crack patterns obtained through the phase-field approach are shown for some states of the load-displacement curve (see Fig. 7b); no difference of the crack pattern arises because of the different fracture energy values,

while a more pronounced sharpness of the crack can be recognized for the lower fracture energy case. As remarked in the previous section, the map of the phase field indicates the existence of a narrow damaged region diffused in the material because of its high deformability.

Finally, Fig. 9 illustrates the phase field map for the polymeric plate for the deformed states indicated with B1 ( $k_d = 0$  Hz), C1, C2 ( $k_d = 0.5$  Hz) and D1, D2, D3 ( $k_d = 0.8$  Hz) of the load-displacement curve reported in Fig. 7c; in all these cases no crack propagation can be noticed, indicating that the high deformability of the polymer reduces the peak stress close to the crack tip, preventing the crack to grow. Moreover, when the viscoelastic behavior is considered, the sensitivity to the crack is less evident, even if no big differences in the crack patterns can be noticed; however, a reduced stress field intensity, induced by the viscoelastic response, entails a significant crack tolerance of the material.

### 5.3. Double edge cracked plate under tension

The last example considers the behavior of a double edge cracked plate under tension. The geometrical and the mechanical characteristics of the cracked plate are the same as those considered above. The plate contains two initial straight edge cracks having dimensionless length  $a/W = 0.3$ , whereas the reciprocal cracks vertical distance has been assumed to be equal to  $b/a = 1$ , and  $b/a = 2/3$ . Both the elastic and the viscoelastic polymeric behavior are considered. The plate made of a strain-dependent polymer (fracture energy  $G_c = 20$  N/m) is studied by considering different viscoelastic degree, namely  $k_d = 0$  Hz,  $k_d = 0.5$  Hz and  $k_d = 0.8$  Hz, while the macroscopic tensile stretch rate applied to the plate has been assumed to be equal to  $\dot{\lambda} = 1.0 \text{ s}^{-1}$ ; the case characterized by  $k_d = 0.8$  Hz has also been studied under a slower stretch rate, i.e.  $\dot{\lambda} = 0.5 \text{ s}^{-1}$ .

Fig. 10a illustrates the geometry and the qualitative deformed shape of the plate under tension, while in Fig. 10b and c shows the dimensionless remote tensile stress vs the dimensionless vertical displacement of the top edge of the plate. For all the examined cases the plate responds in a brittle fashion; however, the polymeric material enables the plate to reach a greater peak load and higher maximum displacements. Higher values of the viscoelastic-related parameter  $k_d$  enable the plate to withstand higher deformations, while for the same strain rate the peak load is not heavily influenced by  $k_d$ ; however, a lower strain rate leads to a failure of the plate for lower maximum deformation.

The phase field map is shown in Fig. 11 for a given stretch value of the plate (points A1, A2, A3 and A4 in Fig. 10c) and for various deformed states taken close to the final collapse of the plate (points B1, B2, B3, B4 in Fig. 10c). The initial upper left crack tends to develop more evidently than the other one because of the unsymmetric boundary condition of the plate.

Also in the present simulations we observe the development of a damage-like narrow region which is characteristic of a highly deformable materials like the polymer here considered. In particular, the case related to the polymer with the largest rate-dependence parameter  $k_d$  and the slowest applied strain rate does not show the development of a clear damaged region (i.e. a less severe damage takes place), because of the stress relaxation allowed by the slow applied load, enabling the material to relax in time more quickly than the applied deformation does.

## 6. Conclusions

The mathematical treatment of problems involving a strong discontinuity in their characterizing field (such as the displacements in mechanics, the concentration in multi-phase problems, etc.) is often a difficult task. In this scenario, the phase-field approach provides a suitable way to reformulate the discontinuous problem by introducing a continuous field variable having the role to smoothly represent the

evolving interface or discontinuity. In the present paper, we have considered the mechanics of polymeric materials – characterized by a high deformability and strain rate dependence – in presence of discontinuities such as in the cases involving the appearance and growth of cracks. The phase-field approach has been developed and generalized to account for the strain rate through a micromechanical model that exploits the concept of chain network rearrangement in time. The micromechanical physics-based theory has been presented and its implementation within the phase-field approach has been discussed. Some examples have been finally illustrated to underline the reliability of the developed computational approach. The role of the viscous behavior, physically corresponding to a stress relaxation of the material, is mainly to smooth out the strong discontinuity arising because of the crack development and growth; a proper tuning of the viscoelastic related parameter allows, at the cost of larger displacements, to control the crack propagation, so providing more crack compliant structures. Further extensions of the micromechanical model, accounting for the stress- and temperature-dependence of the strain rate response of polymers, would be desired to simulate more precisely the response of this class of materials.

## Funding

The author(s) gratefully acknowledge the support of the German Science Foundation (DFG) under the grant. No. 418518589.

## Declaration of competing interest

The authors declare that they have no known competing financial interests or personal relationships that could have appeared to influence the work reported in this paper.

## References

- Amiri, F., Ziae Rad, S., Valizadeh, N., Rabczuk, T., 2019. On the use of local maximum entropy approximants for Cahn–Hilliard phase-field models in 2D domains and on surfaces. *Comput. Methods Appl. Mech. Eng.* 346, 1–24.
- Antanovskii, L.K., 1995. A phase field model of capillarity. *Phys. Fluids* 7 (4), 747–753.
- Barenblatt, G.I., 1962. The mathematical theory of equilibrium cracks in brittle fracture. In: *Adv. Appl. Mech.*, vol. 7. Elsevier, pp. 55–129.
- Bhowmick, S., Liu, G.R., 2018a. Three dimensional cs-fem phase-field modeling technique for brittle fracture in elastic solids. *Appl. Sci.* 8 (12), 2488.
- Bhowmick, S., Liu, G.R., 2018b. A phase-field modeling for brittle fracture and crack propagation based on the cell-based smoothed finite element method. *Eng. Fract. Mech.* 204, 369–387.
- Biben, T., Kassner, K., Misbah, C., 2005. Phase-field approach to three-dimensional vesicle dynamics. *Phys. Rev. E* 72 (4), 041921.
- Biner, S.B., 2017. An overview of the phase-field method and its formalisms. In: *Programming Phase-Field Modeling*. Springer, Cham.
- Borden, M.J., Verhoosel, C.V., Scott, M.A., Hughes, T.J., Landis, C.M., 2012. A phase-field description of dynamic brittle fracture. *Comput. Methods Appl. Mech. Eng.* 217, 77–95.
- Bouchard, P.O., Bay, F., Chastel, Y., Tovena, I., 2000. Crack propagation modelling using an advanced remeshing technique. *Comput. Methods Appl. Mech. Eng.* 189 (3), 723–742.
- Boyce, M., Arruda, E., 2000. Constitutive models of rubber elasticity: a review. *Rubber Chem. Tech.* 73 (3), 504–523.
- Brighenti, R., Artoni, F., Cosma, M.P., 2019. Mechanics of materials with embedded unstable molecules. *J. Sol. Struct.* 162, 21–35.
- Chen, L.Q., 2002. Phase-field models for microstructure evolution. *Annu. Rev. Mater. Res.* 32 (1), 113–140.
- Cristiano, A., Marcellan, A., Long, R., Hui, C.Y., Stolk, J., Greton, C., 2010. An experimental investigation of fracture by cavitation of model elastomeric networks. *J. Polym. Sci. B Polym. Phys.* 48 (13), 1409–1422.
- Doi, M., 1996. *Introduction to Polymer Physics*. Oxford university press.
- Dugdale, D.S., 1960. Yielding of steel sheets containing slits. *J. Mech. Phys. Solid.* 8 (2), 100–104.
- Elices, M.G.V., Guinea, G.V., Gomez, J., Planas, J., 2002. The cohesive zone model: advantages, limitations and challenges. *Eng. Fract. Mech.* 69 (2), 137–163.
- Fixman, M., 1972. *Modern Theory of Polymer Solutions*. Hiromi Yamakawa. Harper and Row, New York, 1971, Harper's Chemistry Series.
- Flory, P.J., 1953. *Principles of Polymer Chemistry*. Cornell University Press.
- Flory, P.J., 1969. *Statistical Mechanics of Chain Molecules*. Wiley-Interscience, New York.
- Flory, P.J., Rehner Jr., J., 1943. Statistical mechanics of cross-linked polymer networks I. Rubberlike elasticity. *J. Chem. Phys.* 11 (11), 512–520.

- Fond, C., 2001. Cavitation criterion for rubber materials: a review of void-growth models. *J Pol. Sci.: Part B: Pol. Physics* 39, 2081–2096.
- Francfort, G.A., Marigo, J.J., 1998. Revisiting brittle fracture as an energy minimization problem. *J. Mech. Phys. Solid.* 46 (8), 1319–1342.
- Gent, A.N., Wang, C., 1991. Fracture mechanics and cavitation in rubber-like solids. *J. Mater. Sci.* 26 (12), 3392–3395.
- Gomez, H., van der Zee, K.G., 2018. Computational Phase-Field Modeling, second ed. Encyclopedia of Comput. Mech., pp. 1–35
- Gordon, M., 1975. The Physics of Rubber Elasticity. L.R.G Treloar, Clarendon Press, Oxford.
- Hansen-Dörr, A.C., Gude, M., Böhm, R., Kästner, M., 2018. Phase-field modelling of fracture in heterogeneous materials. *Proc. Appl. Math. Mech.* 18 (1), e201800082.
- Hofacker, M., Miehe, C., 2012. Continuum phase field modeling of dynamic fracture: variational principles and staggered FE implementation. *J. Fract.* 178 (1–2), 113–129.
- Hui, C.Y., Tang, T., Lin, Y.Y., Chaudhury, M.K., 2004. Failure of elastomeric polymers due to rate dependent bond rupture. *Langmuir* 20 (14), 6052–6064.
- Jacqmin, D., 1999. Calculation of two-phase Navier-Stokes flows using phase-field modeling. *J. Comput. Phys.* 155 (1), 96–127.
- Knauss, W.G., 2015. A review of fracture in viscoelastic materials. *Int. J. Fract.* 196 (1–2), 99–146.
- Kuhn, W., Grün, F., 1942. Beziehungen zwischen elastischen Konstanten und Dehnungsdoppelbrechung hochelastischer Stoffe. *Colloid Polym. Sci.* 101 (3), 248–271.
- Kuhn, C., Müller, R., 2010. A continuum phase field model for fracture. *Eng. Fract. Mech.* 77 (18), 3625–3634.
- Kuhn, C., Müller, R., 2011. A new finite element technique for a phase field model of brittle fracture. *J. Theor. Appl. Mech.* 49 (4), 1115–1133.
- Lev, Y., Volokh, K.Y., 2016. On cavitation in rubberlike materials. *J. Appl. Mech.* 83 (4), 0044501-1–4.
- Lewandowski, R., Chorążycewski, B., 2010. Identification of the parameters of the Kelvin-Voigt and the Maxwell fractional models, used to modeling of viscoelastic dampers. *Comput. Struct.* 88 (1–2), 1–17.
- Li, Y., Hu, S., Sun, X., Stan, M., 2017. A review: applications of the phase field method in predicting microstructure and property evolution of irradiated nuclear materials. *NPJ Comput. Mater.* 3 (1), 16.
- Lin, Y.Y., Hui, C.Y., 2004. Cavity growth from crack-like defects in soft materials. *J. Fract.* 126, 205–221.
- Loew, P.J., Peters, B., Beex, L.A., 2019. Rate-dependent phase-field damage modeling of rubber and its experimental parameter identification. *J. Mech. Phys. Solid.* 127, 266–294.
- Long, R., Qi, H.J., Dunn, M.L., 2013. Modeling the mechanics of covalently adaptable polymer networks with temperature-dependent bond exchange reactions. *Soft Matter* 9 (15), 4083–4096.
- Mandal, T.K., Nguyen, V.P., Wu, J.Y., 2019. Length scale and mesh bias sensitivity of phase-field models for brittle and cohesive fracture. *Eng. Fract. Mech.* 217, 106532.
- May, S., Vignollet, J., De Borst, R., 2015. A numerical assessment of phase-field models for brittle and cohesive fracture:  $\Gamma$ -convergence and stress oscillations. *Eur. J. Mech. Solid.* 52, 72–84.
- Miehe, C., Schänzel, L.M., 2014. Phase field modeling of fracture in rubbery polymers. Part I: finite elasticity coupled with brittle failure. *J. Mech. Phys. Solid.* 65, 93–113.
- Miehe, C., Welschinger, F., Hofacker, M., 2010a. Thermodynamically consistent phase-field models of fracture: variational principles and multi-field FE implementations. *J. Num. Meth. Eng.* 83 (10), 1273–1311.
- Miehe, C., Hofacker, M., Welschinger, F., 2010b. A phase field model for rate-independent crack propagation: robust algorithmic implementation based on operator splits. *Comput. Methods Appl. Mech. Eng.* 199 (45–48), 2765–2778.
- Miura, H., 2018. Phase-field model for growth and dissolution of a stoichiometric compound in a binary liquid. *Phys. Rev. E* 98 (2), 023311.
- Mohammadi, N., Klein, A., Sperling, L.H., 1993. Polymer chain rupture and the fracture behavior of glassy polystyrene. *Macromolecules* 26 (5), 1019–1026.
- Nguyen, T.T., Réthoré, J., Baietto, M.C., 2017. Phase field modelling of anisotropic crack propagation. *Eur. J. Mech. Solid.* 65, 279–288.
- Provatas, N., Elder, K., 2011. Phase-field Methods in Materials Science and Engineering. John Wiley & Sons.
- Schmitz, G.J., 2017. A combined entropy/phase-field approach to gravity. *Entropy* 19 (4), 151.
- Shen, R., Waisman, H., Guo, L., 2019. Fracture of viscoelastic solids modeled with a modified phase field method. *Comput. Methods Appl. Mech. Eng.* 346, 862–890.
- Song, J.H., Fu, Y., Kim, T.Y., Yoon, Y.C., Michopoulos, J.G., Rabczuk, T., 2018. Phase field simulations of coupled microstructure solidification problems via the strong form particle difference method. *J. Mech. Mat. Des.* 14 (4), 491–509.
- Steinbach, I., 2009. Phase-field models in materials science. *Model. Simulat. Mater. Sci. Eng.* 17 (7), 073001.
- Talamini, B., Mao, Y., Anand, L., 2018. Progressive damage and rupture in polymers. *J. Mech. Phys. Solid.* 111, 434–457.
- Teichtmeister, S., Aldakheel, F., Miehe, C., 2016. A Phase-Field Model of ductile fracture at finite strains. *Proc. Appl. Math. Mech.* 16 (1), 181–182.
- Thomas, A.G., 1994. The development of fracture mechanics for elastomers. *Rubber Chem. Technol.* 67 (3), 50–67.
- Torabi, S., Lowengrub, J., Voigt, A., Wise, S., 2009. A new phase-field model for strongly anisotropic systems. *Proc. Math. Phys. Eng. Sci.* 465 (2105), 1337–1359.
- Treloar, L.R.G., 1946. The elasticity of a network of long-chain molecules.— III. *Trans. Faraday Soc.* 42, 83–94.
- Vernerey, F.J., 2018. Transient response of nonlinear polymer networks: a kinetic theory. *J. Mech. Phys. Solid.* 115, 230–247.
- Vernerey, F.J., Long, R., Brighenti, R., 2017. A statistically-based continuum theory for polymers with transient networks. *J. Mech. Phys. Solid.* 107, 1–20.
- Wells, G.N., Sluys, L.J., 2001. A new method for modelling cohesive cracks using finite elements. *J. Num. Meth. Eng.* 50 (12), 2667–2682.
- Wu, P.D., van der Giessen, E., 1993. On improved network models for rubber elasticity and their application to orientation hardening in glassy polymers. *J. Mech. Phys. Solid.* 41, 427–456.
- Wu, J.Y., Nguyen, V.P., 2018. A length scale insensitive phase-field damage model for brittle fracture. *J. Mech. Phys. Solid.* 119, 20–42.
- Yin, B., Kaliske, M., 2020. Fracture simulation of viscoelastic polymers by the phase-field method. *Comput. Mech.* 65 (2), 293–309.
- Yu, F., Wei, Y., Ji, Y., Chen, L.Q., 2018a. Phase field modeling of solidification microstructure evolution during welding. *J. Mater. Process. Technol.* 255, 285–293.
- Yu, K., Xin, A., Wang, Q., 2018b. Mechanics of self-healing polymer networks crosslinked by dynamic bonds. *J. Mech. Phys. Solid.* 121, 409–431.
- Zhang, C., Wang, C., Lahmer, T., He, P., Rabczuk, T., 2016. A dynamic XFEM formulation for crack identification. *J. Mech. Mat. Des.* 12 (4), 427–448.
- Zhou, S., Zhuang, X., Zhu, H., Rabczuk, T., 2018. Phase field modelling of crack propagation, branching and coalescence in rocks. *Theor. Appl. Fract. Mech.* 96, 174–192.